Published online: March 4, 2019

Article

TRANSPARENT PROCESS OPEN ACCESS

THE EMBO JOURNAL

Hfq-dependent mRNA unfolding promotes sRNA-based inhibition of translation

Mirthe Hoekzema, Cédric Romilly, Erik Holmqvist & E Gerhart H Wagner*

Abstract

Small RNAs post-transcriptionally regulate many processes in bacteria. Base-pairing of sRNAs near ribosome-binding sites in mRNAs inhibits translation, often requiring the RNA chaperone Hfq. In the canonical model, Hfq simultaneously binds sRNAs and mRNA targets to accelerate pairing. Here, we show that the *Escherichia coli* sRNAs OmrA and OmrB inhibit translation of the diguanylate cyclase DgcM (previously: YdaM), a player in biofilm regulation. In OmrA/B repression of *dgcM*, Hfq is not required as an RNA interaction platform, but rather unfolds an inhibitory RNA structure that impedes OmrA/B binding. This restructuring involves distal face binding of Hfq and is supported by RNA structure mapping. A corresponding mutant protein cannot support inhibition *in vitro* and *in vivo*; proximal and rim mutations have negligible effects. Strikingly, OmrA/B-dependent translational inhibition *in vitro* is restored, in complete absence of Hfq, by a deoxyoligoribonucleotide that base-pairs to the biochemically mapped Hfq site in *dgcM* mRNA. We suggest that Hfq-dependent RNA structure remodeling can promote sRNA access, which represents a mechanism distinct from an interaction platform model.

Keywords biofilm; Hfq; post-transcriptional regulation; RNA structure; sRNA
Subject Categories Microbiology, Virology & Host Pathogen Interaction; RNA Biology
DOI 10.15252/embj.2018101199 | Received 19 November 2018 | Revised 5 February 2019 | Accepted 6 February 2019
The EMBO Journal (2019) e101199

Introduction

Bacterial antisense RNAs were initially found and described as regulators in accessory elements: plasmids, phages, and transposons (Wagner *et al*, 2002; Wagner & Romby, 2015). These *cis*-encoded antisense RNAs are encoded overlapping—in opposite orientation—their single target genes and thus have complete complementarity (Waters & Storz, 2009; Wagner & Romby, 2015; and references therein). Subsequently, numerous chromosomally encoded so-called small RNAs (sRNAs) were discovered and are part of a large repertoire of post-transcriptional regulators in all bacteria and archaea (Beisel & Storz, 2010; Gottesman & Storz, 2011; Barquist & Vogel, 2015; Wagner & Romby, 2015; Holmqvist & Wagner, 2017). This heterogeneous class of RNAs impacts on global regulatory circuits in metabolism, virulence, stress responses, and motility/biofilm formation decisions. A striking feature involves targeting of multiple genes within the same network. This relies on properties of *trans*-encoded sRNAs: Since many sRNA genes do not overlap with target genes, base-pairing is non-contiguous and limited. Bacterial sRNAs can promote translational activation or, more frequently, repression (Papenfort & Vanderpool, 2015; Wagner & Romby, 2015; Carrier *et al*, 2018). Furthermore, target mRNAs can become stabilized or undergo facilitated decay (Lalaouna *et al*, 2013; Papenfort *et al*, 2013).

In many but not all bacteria, *trans*-encoded sRNAs require the RNA chaperone Hfq for efficient regulation (Vogel & Luisi, 2011; Holmqvist & Vogel, 2018; Woodson *et al*, 2018). Hfq is a ring-like homohexamer with at least three distinct RNA-binding surfaces (Updegrove *et al*, 2016; Santiago-Frangos & Woodson, 2018). The distal face of *Escherichia coli* Hfq recognizes A-rich sequences, or $(AAN)_n$ motifs, and primarily binds mRNAs (Link *et al*, 2009; Robinson *et al*, 2014). In contrast, most sRNAs bind the proximal face via the poly-U tails of their Rho-independent terminators (Otaka *et al*, 2011; Ishikawa *et al*, 2012), with specific recognition of the 3′ hydroxyl group (Sauer & Weichenrieder, 2011). Additional contacts are provided between internal U/A sequences and arginine patches on the lateral binding surface/rim (Sauer *et al*, 2012). Enterobacterial Hfq also carries intrinsically disordered C-terminal domains (CTD; Beich-Frandsen *et al*, 2011) whose function has been controversial. CTDs may aid recruitment of sRNAs, specifically RydC, to Hfq (Dimastrogiovanni *et al*, 2014). A recent study suggests their importance for the rapid release of bound RNAs (Santiago-Frangos *et al*, 2016). Overall, Hfq is regarded as a platform on which RNAs meet for interaction. For this to happen on a biologically relevant timescale, RNAs must rapidly exchange on the limiting Hfq pool. RNA concentration-driven cycling on Hfq has strong support from *in vitro* and *in vivo* experiments (Fender *et al*, 2010; Salim & Feig, 2010; Hussein & Lim, 2011; Moon & Gottesman, 2011; Olejniczak, 2011; Wagner, 2013).

Interaction with Hfq protects many RNAs from rapid degradation (Moll *et al*, 2003a; Holmqvist *et al*, 2010) and promotes the annealing of sRNAs and their mRNA targets (Møller *et al*, 2002; Zhang *et al*, 2002; Lease & Woodson, 2004; Fender *et al*, 2010; Wroblewska & Olejniczak, 2016). Several non-exclusive models

Department of Cell and Molecular Biology, Biomedical Center, Uppsala University, Uppsala, Sweden
*Corresponding author. Tel: +46 18 471 4866; Fax: +46 18 530396; E-mail: gerhart.wagner@icm.uu.se

suggest how Hfq can facilitate intermolecular base-pairing. Simultaneous binding of two RNA molecules to an Hfq hexamer could help their interaction through "molecular crowding" (Rajkowitsch & Schroeder, 2007). Hfq binding may also entail structural rearrangements in RNAs, to unfold an otherwise inaccessible seed sequence in an sRNA (Zhang *et al*, 2002; Gorski *et al*, 2017) or possibly a sequestered target sequence in an mRNA. The latter has previously been proposed for *sodB* mRNA (Geissmann & Touati, 2004), but, as will be detailed in the Discussion, lacks unambiguous experimental support and has been challenged (Hao *et al*, 2011). Another mechanism specifically moves the seed region of an sRNA into close proximity to its complement in the mRNA (Vogel & Luisi, 2011; Gorski *et al*, 2017). For example, the *rpoS* mRNA folds around Hfq, through contacts with distal and rim surfaces, into a compact ternary structure that positions the base-pairing region adjacent to the complementary site within the sRNA DsrA (Peng *et al*, 2014a,b). Interaction with the Hfq rim can also position sRNAs for optimal base-pairing, as shown for RydC-*cfa* (Dimastrogiovanni *et al*, 2014). Besides positioning RNAs for interaction, the conserved arginine patches on the Hfq rim apparently play a role in duplex formation by overcoming electrostatic barriers to helix nucleation (Panja *et al*, 2013, 2015).

We and others have been interested in two sequence-similar sRNAs, OmrA and OmrB, which act on multiple target mRNAs to regulate outer membrane and surface protein expression (Guillier & Gottesman, 2006, 2008; Holmqvist *et al*, 2010; Mika & Hengge, 2014; Brosse *et al*, 2016; Jagodnik *et al*, 2017). Their genes (Argaman *et al*, 2001; Wassarman *et al*, 2001; Vogel *et al*, 2003) are transcriptionally activated by the OmpR-EnvZ two-component system, e.g., under high osmolarity conditions (Guillier & Gottesman, 2006; Brosse *et al*, 2016). OmrA, but not OmrB, is additionally under the control of the stress sigma factor σ^s (*rpoS*; Lévi-Meyrueis *et al*, 2014; Peano *et al*, 2015; Colgan *et al*, 2016). Both sRNAs associate with Hfq *in vitro* (Holmqvist *et al*, 2010) and *in vivo* (Wassarman *et al*, 2001; Zhang *et al*, 2003; Chao *et al*, 2012; Tree *et al*, 2014; Holmqvist *et al*, 2016); the sRNAs are destabilized in Δ*hfq* cells (Holmqvist *et al*, 2010). OmrA and OmrB are redundant on most targets, using their almost identical 5′ tails for base-pairing. Some validated target mRNAs encode the outer membrane proteins CirA and OmpT, their own activator OmpR (Guillier & Gottesman, 2008), the flagellar regulator FlhD (De Lay & Gottesman, 2012), and CsgD (Holmqvist *et al*, 2010), the master transcriptional activator of the genes for the biofilm components curli and cellulose (Hammar *et al*, 1995; Römling, 2005). The regulation of *csgD* by OmrA and OmrB (Holmqvist *et al*, 2010) and by four subsequently reported sRNAs (Jørgensen *et al*, 2012; Mika *et al*, 2012; Thomason *et al*, 2012; Bordeau & Felden, 2014) has highlighted the importance of tight regulation of biofilm formation. In addition to post-transcriptional control by sRNAs, *csgD* expression is extensively regulated at the level of transcription, e.g., by the OmrAB-regulated transcription factor OmpR, and DgcM (previously: YdaM; Hengge *et al*, 2015; Fig 1A). DgcM, a c-di-GMP-producing diguanylate cyclase (DGC), is part of a c-di-GMP-dependent switching module involved in the signaling cascade that controls curli synthesis. The phosphodiesterase (PDE) PdeR (a.k.a. YciR) directly inhibits DgcM until the levels of the second messenger c-di-GMP are sufficient for it to function as a PDE. DgcM then produces more c-di-GMP and, through a double-negative feedback loop, activates MlrA (Lindenberg *et al*, 2013). DgcM, MlrA, and σ^s are all required for transcription of *csgD*. CsgD in turn activates transcription of the c*sgBAC* operon that encodes curli proteins (Hammar *et al*, 1995; Fig 1A).

In this study, we identified *dgcM* as an additional OmrA/B target, upstream in the curli/biofilm pathway. Unexpectedly, our results

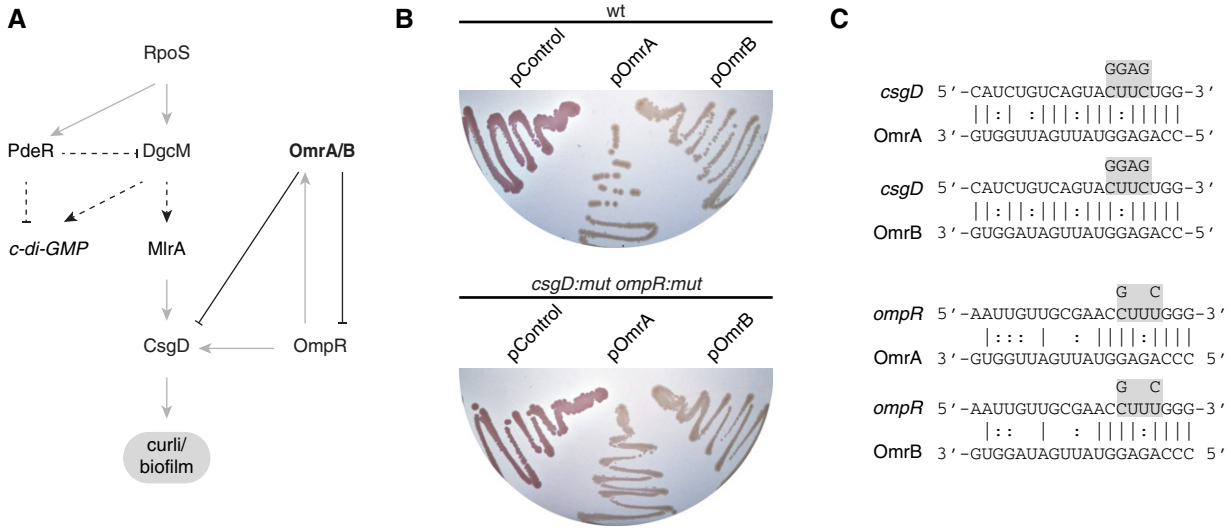

Figure 1. A new OmrA and OmrB target, in addition to *csgD* and *ompR*, that affects curli synthesis.

A Schematic overview of part of the biofilm regulatory network, highlighting the roles of OmrA and OmrB. Gray arrows: transcriptional activation, black lines with bars: post-transcriptional negative regulation, dotted lines: direct protein–protein or protein–c-di-GMP interactions.

B Congo red plates with colonies of *Escherichia coli* strain MC4100 *relA*$^+$ and its target mutation *csgD:M4–ompR:mut2* derivative, harboring sRNA-producing plasmids pOmrA, pOmrB, or an empty vector (pControl). Incubation at 28°C for 48 h.

C Schematic showing published interaction sites between OmrA or OmrB and targets *csgD* or *ompR* (Guillier & Gottesman, 2008; Holmqvist *et al*, 2010). Mutations introduced to disrupt base-pairing are in gray boxes.

suggest a new mechanism by which Hfq promotes regulation. Here, rather than acting canonically as a platform for simultaneous interactions that facilitate sRNA-mRNA pairing, Hfq is primarily needed to render the mRNA target accessible for sRNA binding.

Results

OmrA and OmrB have multiple targets in the same regulatory pathway

We previously showed that OmrA/B inhibit the synthesis of CsgD (Holmqvist *et al*, 2010). OmrA/B also repress the synthesis of OmpR (Guillier & Gottesman, 2008), a transcriptional activator of *csgD* (Römling *et al*, 1998; Vidal *et al*, 1998; Prigent-Combaret *et al*, 2001; Gerstel *et al*, 2003; Ogasawara *et al*, 2010; Fig 1A). As a result of the dual repression of these biofilm activators, ectopic overexpression of OmrA or OmrB downregulates curli production, resulting in white colonies on Congo red indicator plates (Holmqvist *et al*, 2010; Fig 1B). In an attempt to render curli production independent of OmrA/B, we introduced chromosomal point mutations in *csgD* and *ompR* mRNAs that disrupt base-pairing with both sRNAs (Guillier & Gottesman, 2008; Holmqvist *et al*, 2010; Fig 1C). Surprisingly, these mutations failed to suppress the OmrA/B-dependent inhibition of curli production, as overexpression of the sRNAs still gave white colonies on the indicator plates (Fig 1B and Appendix Fig S1). This suggested that OmrA/B may inhibit curli formation not only through *csgD* and *ompR*, but also other targets.

OmrA and OmrB inhibit DgcM synthesis through direct base-pairing interactions

Computational predictions of base-pairing between OmrA or OmrB and mRNAs from biofilm-associated genes (IntaRNA algorithm; Busch *et al*, 2008) indicated an interaction between the 5′-tails of OmrA/OmrB and nucleotides 91–102 of *dgcM* mRNA (Fig 2A). To assess whether OmrA and/or OmrB can inhibit *dgcM* expression, fluorescence of cells harboring a plasmid encoding a *dgcM::gfp* translational fusion was measured in the presence and absence of plasmids encoding *omrA* or *omrB*. Overexpression of either of the sRNAs strongly decreased fluorescence compared to an empty vector control (Fig 2B), indicating direct repression of DgcM synthesis by the sRNAs. When the same plasmids were introduced into a Δ*hfq* background, regulation was lost (Fig 2B). Note, however that, as for *csgD* (Holmqvist *et al*, 2010), uninhibited *dgcM* expression was ≈3-fold lower in a Δ*hfq* than an *hfq*$^+$ background (Appendix Fig S2A). Thus, as in many *trans*-encoded sRNA–target interactions, Hfq is required for regulation. To assess whether inhibition of *dgcM* is dependent on the predicted base-pairing interaction, Western blot analysis was performed on cell lysates from *E. coli* cells expressing *dgcM* with a C-terminal 3xFLAG sequence, combined with OmrA or OmrB overexpression vectors, or their mutant variants OmrA_M2, OmrB_M2 (Fig 2A). Overexpression of wild-type (wt) OmrA or OmrB strongly decreased DgcM-3xFLAG signals, congruent with the GFP fusion results (Fig 2B and C). As expected, mismatched OmrA_M2 or OmrB_M2 did not affect DgcM expression, supporting the importance of these nucleotides in base-pairing to the *dgcM* mRNA (Fig 2A and C). A compensatory mutation in *dgcM*, designed to base-pair with OmrA_M2 and OmrB_M2, restored regulation for OmrB_M2, but not OmrA_M2 (Fig 2A and C). Mobility shift assays showed binding of OmrA_M2 to both the wt *dgcM* and *dgcM_M2* mRNAs (Appendix Fig S3). We therefore hypothesize that OmrA_M2 preferably binds to a second, likely regulatorily inert site. Interestingly, when we supplemented a strain carrying both *csgD* and *ompR* target mutations (Fig 1C) with a plasmid encoding *dgcM-M2*, thus rendering all known OmrA/B biofilm targets unregulated, biofilm formation was restored in the presence of OmrA, but not OmrB (Appendix Fig S4A). It is therefore possible

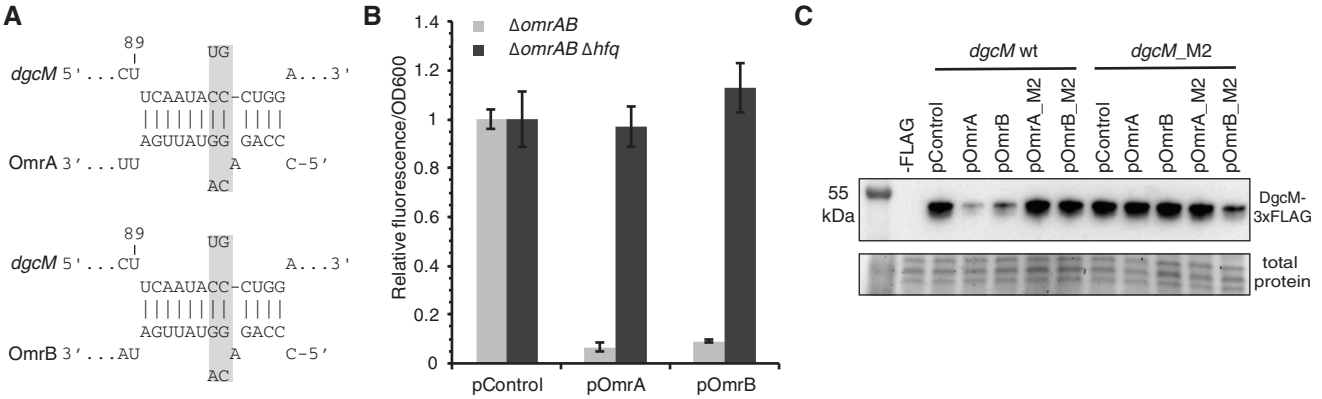

Figure 2. OmrA and OmrB inhibit *dgcM* expression *in vivo* by direct base-pairing in an Hfq-dependent manner.

A Predicted base-pairing between *dgcM* mRNA and OmrA/OmrB. Gray boxes show the M2 point mutation introduced to disrupt the interaction. The UTR is 74 nt long (to AUG), and the interaction site is numbered.

B Relative fluorescence/OD_{600} of cells of *Escherichia coli* strain MC4100 *relA*$^+$ Δ*omrAB* or MC4100 *relA*$^+$ Δ*omrAB* Δ*hfq* harboring the translational fusion plasmid pDgcM::GFP in combination with plasmids expressing OmrA, OmrB, or an empty control vector, after 16 h of growth at 37°C. Error bars SD, $N = 3$. Average fluorescence intensities (a.u.)/OD_{600} used to calculate ratios can be found in Appendix Fig S2A. Note that absolute *dgcM::gfp* expression values are ≈3–4-fold lower in the Δ*hfq* strain (Appendix Fig S2B).

C Western blot analysis of cell lysates from strains MC4100 *relA*$^+$ Δ*omrAB* harboring plasmids pOmrA, pOmrB, or mutant variants as indicated, in combination with a plasmid expressing C-terminal FLAG-tagged *dgcM* or *dgcM_M2*. As a loading control, part of a protein-stained gel is shown below.

that OmrB may target additional biofilm-related mRNAs. Taken together, our results indicate that OmrA and OmrB repress DgcM output by direct base-pairing interaction within the early coding region of the mRNA and that Hfq is required for their effect.

OmrA and OmrB inhibit *dgcM* translation *in vitro*

The OmrA/OmrB interaction site on *dgcM* is located immediately downstream of the "5-codon window" within which sRNAs are believed to interfere with 30S ribosomal subunit binding (Bouvier *et al*, 2008). Thus, we tested whether OmrA and OmrB can block initiation complex formation on *dgcM* mRNA. As expected, a characteristic 30S/$tRNA_{fMet}$-dependent reverse transcription stop ("toeprint") at position +15 was observed, which was absent upon inclusion of OmrA or OmrB (Fig 3A); an unrelated sRNA, IstR-1 (Vogel *et al*, 2004), failed to inhibit the *dgcM* toeprint.

Translational level regulation was further tested with *in vitro* assays. Here, *dgcM::FLAG* and *ompA::FLAG* mRNAs were used as templates, the latter serving as internal control; this mRNA is not subject to OmrA/B regulation. Upon adding OmrA or OmrB to the reaction, a slight reduction of DgcM translation was observed, with OmrA being reproducibly more effective than OmrB (Fig 3B). Addition of Hfq greatly enhanced the inhibitory effect of both sRNAs, so that DgcM was essentially absent (Fig 3B). *In vivo*, Hfq is required for the stability of OmrA and OmrB (Holmqvist *et al*, 2010). However, since RNAs are entirely stable in the PURExpress® *In Vitro* Protein Synthesis Kit (Sharma *et al*, 2007), this striking regulatory dependence implies a key role for Hfq in *dgcM* mRNA-OmrA/B duplex formation.

OmrA/B and *dgcM* mRNA interaction sites

The above results suggest that *dgcM* mRNA and OmrA/B directly base-pair with each other, most likely in close proximity of, or overlapping, the ribosome-binding site (RBS). To precisely map this interaction, a footprinting analysis was conducted by enzymatic and chemical probing. 5′-end-labeled *dgcM* mRNA, ±Hfq, and/or OmrA/B was subjected to limited digestion (on average < 1 cut/RNA molecule) with RNase T1 (specific for unpaired G residues) or lead(II) acetate (specific for single-stranded nucleotides; Fig 4A). Binding of Hfq alone protected residues 48–64 (lead-II cleavage) as well as G54 (RNase T1; Fig 4A and B). This region of the *dgcM* mRNA features the typical $(AAN)_n$ motifs known to bind the distal face of Hfq hexamers (Link *et al*, 2009; Robinson *et al*, 2014). Hfq binding also induced minor long-range structural rearrangements, e.g., 5′ of the main Hfq-binding site (G32–G39; Fig 4A). Importantly, Hfq binding entailed an opening of the small hairpin that contains the RBS of the *dgcM* mRNA, indicated by enhanced T1 cuts of G66–68 within the SD sequence, and at G83 on the opposite side of the stem. We also observed that residues G101 and G102 showed slightly increased accessibility toward RNase T1 (Fig 4A, lane 6). Unexpectedly, structural probing done with Hfq and either OmrA or OmrB revealed the presence of two adjacent sRNA-binding sites (Fig 4A, lanes 9–10, and 15–16, indicated by red and blue boxes). Protection of site 1 was identical for both OmrA and OmrB and concurred with the computationally predicted binding site. It spans from position U91 to G102, as shown by complete protection of G101 and G102 from T1 cleavage, and lead-II protection from U91 to G102 (Fig 4A and B). Site 2 differs between the sRNAs. Both OmrA and OmrB base-pair from U121 to G125, since G124, G125 (T1), and U121 to G125 (lead-II) were fully protected in the presence of Hfq and the sRNAs (Fig 4A, lanes 9–10). Binding of OmrA, but not OmrB, extended protection to residues C110 to U123 (lead-II) and G115 (T1). Incidentally, both OmrA/B binding sites are supported by RIL-seq results (Melamed, personal communication; Melamed *et al*, 2016). Corresponding and complementary probing was done with labeled OmrA and OmrB (Appendix Fig S5). As expected, both sRNAs bind through their conserved 5′ tails, as seen on other mRNA targets (Holmqvist *et al*, 2010).

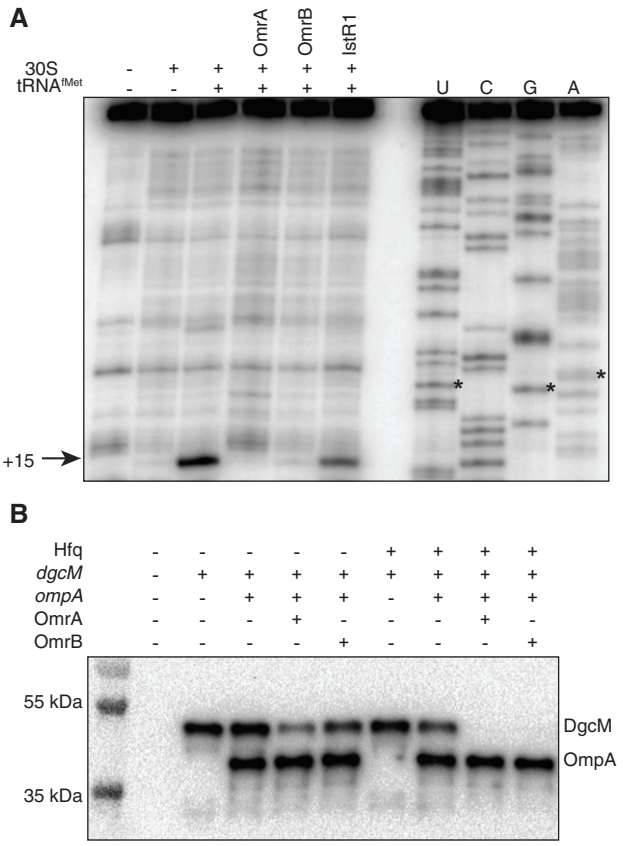

Figure 3. OmrA/B inhibit DgcM translation by competing for ribosome binding.

A Toeprinting showing inhibition of initiation complex formation on a truncated *dgcM* mRNA (210 nt from +1) by OmrA and OmrB. Inclusion of 30S ribosomes, $tRNA_{fmet}$, OmrA, and OmrB is indicated. The unrelated IstR-1 sRNA is a negative control. The 30S/$tRNA_{fmet}$-dependent reverse transcription block (toeprint) is indicated by an arrow. Sequencing reactions were loaded next to the primer extension products (UCGA). The AUG start codon is indicated by asterisks.

B *In vitro* translation of *dgcM::3xflag* mRNA in the presence or absence of OmrA/OmrB, with or without purified Hfq protein, was carried out as in Materials and Methods. As an internal control, the non-target *ompA::3xflag* mRNA was included. The Western blot shows DgcM-3xFLAG and OmpA-3xFLAG protein levels.

To confirm OmrA/B binding to sites 1 and 2, we performed mobility shift assays with a shorter end-labeled *dgcM* mRNA and OmrA or OmrB. DNA-oligos complementary to site 1 or site 2 (Appendix Fig S6 and Table S1) were pre-annealed to the mRNA to

Published online: March 4, 2019

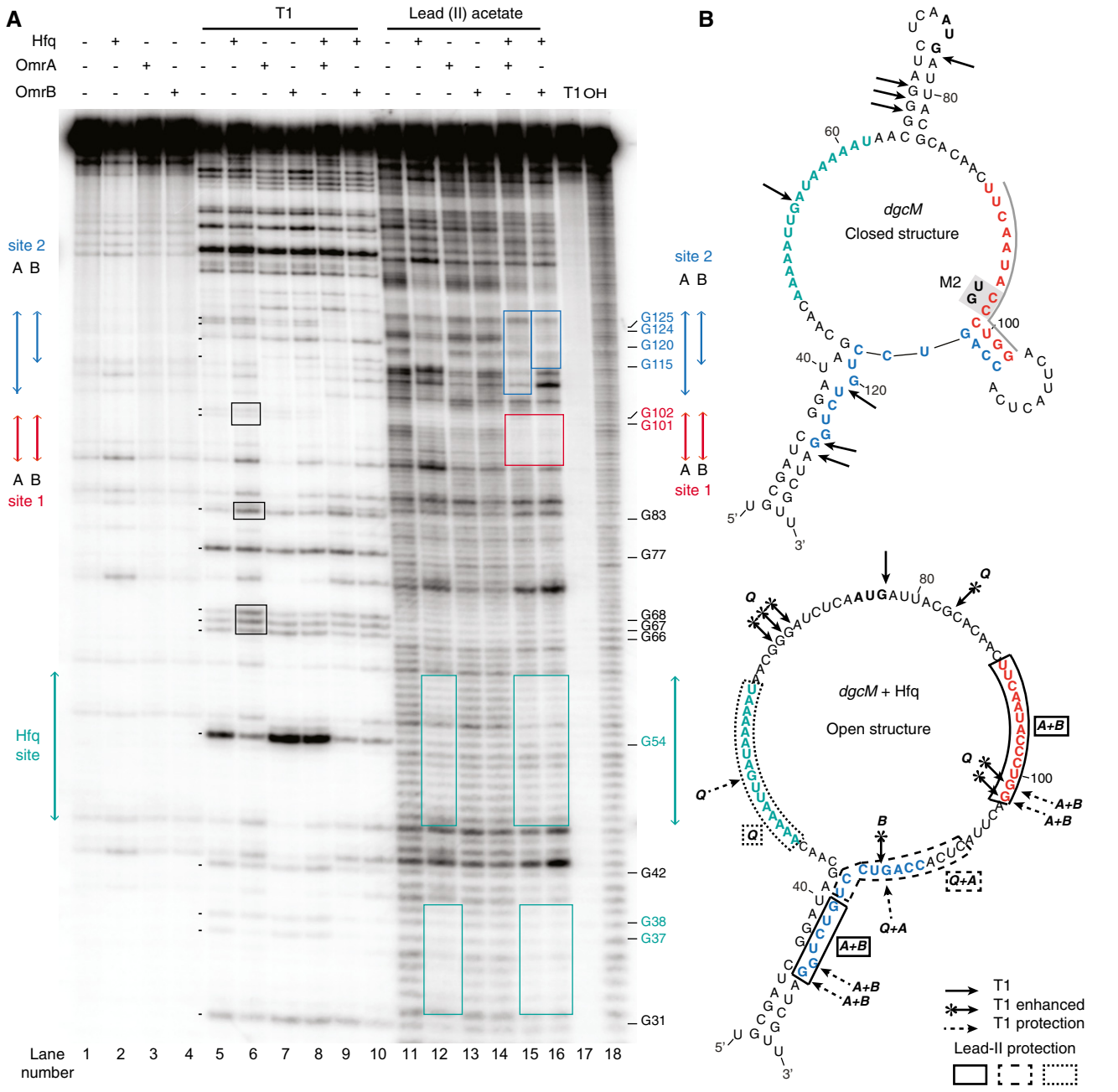

Figure 4. Footprinting of the OmrA/OmrB/Hfq-binding sites on *dgcM* mRNA by chemical and enzymatic probing.

A 5′ end-labeled *dgcM* mRNA (10 nM) was subjected to probing as described in Materials and Methods. All components added to the labeled RNA are indicated above the autoradiogram. When added, Hfq hexamers were at 50 nM, the sRNAs OmrA and OmrB at 250 nM. The accessibility of each nucleotide was probed with water (lanes 1–4, negative control for RNA integrity), RNase T1, or lead(II) acetate. Lane T1: RNase T1 under denaturing conditions. Lane OH: alkaline ladders. Binding sites of Hfq (green arrows and boxes), and site 1 (red arrows and boxes) and 2 (blue arrows and boxes) of the sRNAs, are highlighted. Note that site 2 is bound differently by OmrA and OmrB (blue boxes on gel). Black boxes indicate Hfq-dependent T1 cleavage enhancements.

B Secondary structure of *dgcM* mRNA ± Hfq, based on results in (A). Nucleotides are color-coded as in (A). Unchanged T1 cleavages are indicated by filled arrows, enhanced T1 cleavages by arrow and star, protection from T1 cleavages by dashed arrows. Lead(II) acetate-protected sequences are indicated by full (Hfq + OmrA/B), dashed (Hfq + OmrA), or dotted (Hfq alone) frames. In the lower panel, Q = Hfq, A = OmrA, and B = OmrB.

block the accessibility of the respective sites to base-pairing of the sRNAs. When site 1 was blocked, OmrA—but not OmrB—could still bind site 2 (Fig 5). Blocking site 2 still permitted both sRNAs to bind site 1. When both sites were blocked, neither of the sRNAs could bind. Interestingly, in the absence of oligos, OmrA was more efficient in the gelshift than OmrB. Furthermore, a super-shift was observed with OmrA-*dgcM* mRNA, indicating that two OmrA molecules were bound to one *dgcM* mRNA. Though binding between OmrA and site

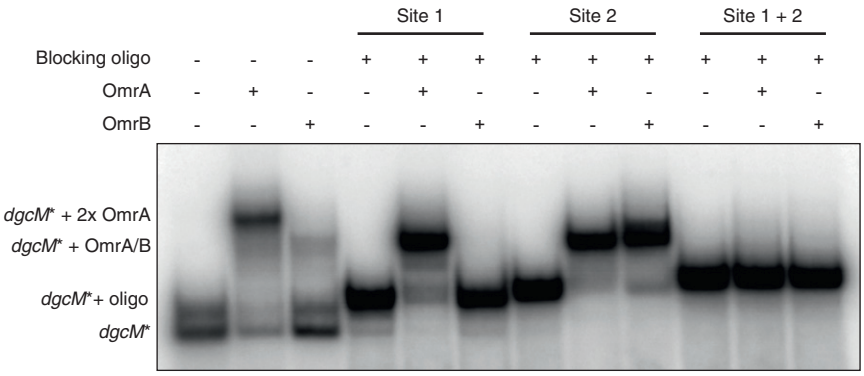

Figure 5. DNA-oligo binding to *dgcM* mRNA blocks OmrA and OmrB access.

Mobility shift assay with end-labeled *dgcM* RNA (210-nt species from +1) in the presence or absence of unlabeled OmrA or OmrB. When indicated, single-stranded DNA-oligos were pre-annealed to site 1 (dgcM_site1), site 2 (dgcM_site2), or both, before addition of sRNAs. For locations of the binding sites, see Appendix Fig S6. The additions for each sample are indicated above the Figure, and the identities of the nucleic acid complexes are indicated on the left for guidance.

2 clearly occurs *in vitro* (Figs 4 and 5), this interaction is likely not of regulatory importance, since point mutations introduced in site 1 alone eliminated regulation completely (Fig 2A and C).

Hfq-dependent restructuring of the *dgcM* mRNA is essential for regulation by OmrA and OmrB

Inspection of the predicted *dgcM* 5′ structure based on footprinting results (Fig 4) and the mFold algorithm (Zuker, 2003) suggested that the presumed seed region within the OmrA/B binding site 1 is partially sequestered in a hairpin (Fig 4B, upper structure), likely rendering it difficult to access by the sRNAs. Based on footprinting results (Fig 4A), we hypothesized that Hfq binding unfolds this structure to facilitate sRNA-mRNA duplex formation (Fig 4B, lower structure). If so, this might explain the strong dependence on Hfq for regulation. However, Hfq is also known to enhance base-pairing rates by bringing sRNA and mRNA target into close proximity, since it can bind two RNAs simultaneously through its different interaction surfaces. To tease apart the contributions of Hfq in these non-exclusive models, we performed translation assays, adding Hfq mutant proteins with specific impairments in the proximal (St_Hfq102_F42A), distal (St_Hfq102_Y25A_Q52A), or rim (St_Hfq 102R16S_R17A_R19A_K47E) interaction surface (Sauer *et al*, 2012); the Hfq mutant proteins are subsequently referred to as Hfq-dist, Hfq-prox, and Hfq rim. As in Fig 3B, *ompA* mRNA was used as an OmrA/B-independent internal control.

Figure 6A shows that, at the concentrations used, OmrA or OmrB alone do not significantly inhibit DgcM translation, whereas the inclusion of wt Hfq drives DgcM output down to barely detectable levels. The *dgcM* mRNA, carrying an A-rich Hfq-binding motif (+45–65, Fig 4B), is expected to interact with the Hfq distal face (Link *et al*, 2009). Assuming that Hfq-mediated opening of the inhibitory structure in *dgcM* mRNA is important for OmrA/B binding, mutations affecting the distal face should impair regulation. Indeed, supplementing the *in vitro* translation reaction with a distal face mutant protein strongly impeded OmrA-dependent regulation, nearly mirroring the absence of Hfq (Fig 6A). In agreement, mobility shift assays showed that, in the presence of Hfq-dist, very little *dgcM*-OmrA complex was formed (Appendix Fig S7). By contrast, Hfq-prox or Hfq rim supported strong inhibition by OmrA, and less so by OmrB. Hence, these surfaces are not strictly needed for Hfq's regulation-enhancing effect, whereas distal face interaction on *dgcM* mRNA is required for efficient regulation.

The results in Fig 6A alone do not exclude a simultaneous interaction of either sRNA with Hfq as important for regulation. However, since the proximal face and rim are preferred interaction surfaces for most sRNAs, including OmrA and OmrB (Schu *et al*, 2015), Hfq-prox and Hfq rim should not interact with the sRNAs, but be still capable of opening the inhibitory structure in *dgcM* mRNA. Mobility shift assays confirmed that OmrA does not bind to Hfq rim but forms a complex with Hfq-prox (Appendix Fig S7). This indicates that for OmrA, akin to some sRNAs like RyhB and RprA, the rim suffices for stable interaction (Sauer *et al*, 2012). More importantly, Hfq rim, unable to bind OmrA (Appendix Fig S7), nevertheless supports strong OmrA-dependent inhibition of DgcM translation (Fig 6A), suggesting that Hfq rim acts here through its intact distal face, similar to Hfq-wt. Mobility shift assays indeed show Hfq rim promoted OmrA-*dgcM* mRNA complex formation, but—unlike with Hfq-wt and Hfq-prox—no slowly migrating ternary complexes (Appendix Fig S7). Taken together, Hfq distal face binding to *dgcM* mRNA is most important for regulation, whereas binding of Hfq to OmrA/B, and its effect on annealing, may be less important or not required.

Forced opening of the inhibitory structure is sufficient to enhance regulation

Based on the above results, a forced opening of the structure that hinders OmrA/B access might bypass the Hfq requirement. We chose to mimic Hfq binding by annealing of a DNA-oligo with complementarity to the Hfq-binding site in *dgcM* (Appendix Table S1 and Fig S6). Indeed, a *dgcM* mRNA annealed to the Hfq-mimic oligo was substantially inhibited by both OmrA and OmrB in the complete absence of Hfq (Fig 6B). The inhibition by OmrA/B was roughly comparable to that obtained in the presence of Hfq (cf. Fig 6B and A, lanes 4–6) and significantly stronger than in its absence (Fig 6A, lanes 1–3). Altogether, this suggests that—in the case of OmrA/B regulation of *dgcM*—an "interaction platform" involving the binding of both interacting RNAs is not required. Rather, the major role of Hfq lies in converting

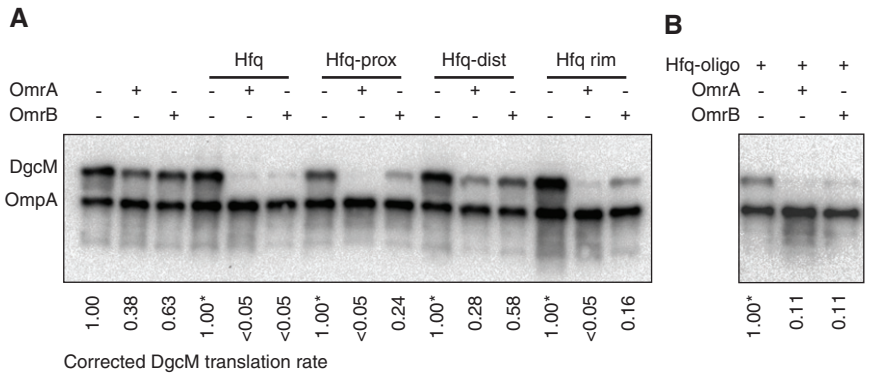

Figure 6. Effects of mutant or wild-type Hfq variants, and of an Hfq-mimic oligo, on OmrA/B regulation of DgcM translation *in vitro*.

Western blots showing DgcM-3xFLAG translated *in vitro* in the presence or absence of OmrA or OmrB.

A The inclusion of purified wild-type or mutant Hfq proteins is indicated, and the translation assay was conducted as in Materials and Methods. The different Hfq interaction site mutant proteins are indicated.

B An ssDNA-oligo (Hfq_BS, Appendix Table S1) that base-pairs specifically to the Hfq-binding site on *dgcM* mRNA (nt 42–66) was pre-annealed to the mRNA prior to OmrA/B addition and translation. OmpA-3xFLAG was included as internal control.

Data information: Quantification of DgcM translation rates, relative to that of the unaffected OmpA control, is shown below the gels. The ratio of DgcM/OmpA signal was set to unity for the lane lacking sRNA in each set of three combinations (−sRNA, +OmrA, +OmrB), indicated by "1.00*". Effects due to OmrA/OmrB addition can be seen by comparing lanes 2 and 3 to lane 1 in each set.

an mRNA structure element into an sRNA-accessible site (cf. structures in Fig 4B). This inference predicts that OmrA/B association rates should be higher upon structure opening. Mobility shift assays with labeled OmrA and *dgcM* mRNA, or *dgcM* mRNA with the pre-annealed mimic oligo, indeed showed association rates effects; second-order binding rate constants for OmrA to *dgcM* were about three times higher in presence of the oligo (Appendix Fig S8).

In conclusion, the Hfq requirement for regulation can be largely bypassed by binding of a DNA-oligo that opens a local structure in the *dgcM* mRNA. Thus, the predominant function of this RNA chaperone lies in unfolding *dgcM* mRNA to render its target region more rapidly accessible to OmrA/B.

The Hfq distal surface is required for OmrA/B-dependent regulation of DgcM *in vivo*

To assess the contribution of the Hfq-binding surfaces on regulation *in vivo*, we introduced the *dgcM::gfp* translational fusion plasmid into *E. coli* strains harboring chromosomal *hfq*-F42A, *hfq*-Y25D, *hfq*-R16S_R17A_R19A_K47E mutant alleles, as well as in a wild-type and a Δ*hfq* strain. Flow cytometric analyses of these cells, carrying or lacking *omrA* or *omrB* expression plasmids, showed that—in line with Fig 2—regulation was abolished in a Δ*hfq* background. Interestingly, regulation was also lost in the distal face mutant (*hfq*-Y25D) strain (Fig 7A), in spite of even slightly higher sRNAs levels than in the wild-*type hfq* strain (Fig 7B; cf. *hfq* wt and *hfq*-dist). These results are congruent with the *in vitro* experiment in Fig 6A and support that the Hfq distal face is required for remodeling of the *dgcM* mRNA and regulation also in an intracellular environment. In apparent contrast to the *in vitro* translation experiment (Fig 6A), *hfq* proximal and rim mutations fail to support regulation of *dgcM* by OmrA and OmrB *in vivo* (Fig 7A). This is however tentatively explained by the strongly reduced stability of the sRNAs in these mutant strains (Fig 7B).

In conclusion, the distal face of the Hfq hexamer is essential for OmrA/B-dependent regulation of *dgcM* both *in vitro* and *in vivo*. This likely reflects that the Hfq distal surface interaction with the *dgcM* mRNA promotes local unfolding, exposing the seed region for OmrA and OmrB interaction and facilitating sRNA-mRNA duplex formation.

Discussion

In this report, we identified *dgcM*, encoding an upstream regulator of the biofilm signaling pathway in *E. coli*, as a target of the sRNAs OmrA and OmrB, thus adding to the complexity of the sRNA network in control of biofilm formation (Boehm *et al*, 2010; Fig 1A). As suggested by Mika and Hengge (2013, 2014), OmrA/B regulation of *dgcM*, as well as *csgD*, might be important to prevent expression of biofilm components under stationary-phase conditions where RpoS is active, and may be critical in the decision to convert from a motile planktonic to a biofilm lifestyle. Inhibition of DgcM translation *in vivo* and *in vitro* occurs by direct base-pairing within the early coding region, as defined by effects of mutations in site 1 (Fig 2). Though OmrA/B pulse expression causes a strong decrease in *dgcM* mRNA levels (Hoekzema, Holmqvist, in preparation), the demonstration that the sRNAs inhibit initiation complex formation (Fig 3A) and *in vitro* translation (Fig 3B) indicates translation inhibition to be the dominant effect. As is true for many other sRNA-mRNA combinations, regulation of *dgcM* by OmrA/B is dependent on the RNA chaperone Hfq. This applies not only *in vivo*, where Hfq is needed to stabilize these sRNAs (Holmqvist *et al*, 2010), but also *in vitro* (Fig 6A) where stabilization effects are ruled out.

Enzymatic and chemical structure probing of the *dgcM* mRNA combined with *in silico* structure predictions (mFold; Zuker, 2003) indicated that OmrA/B binding site 1, on which regulation depends

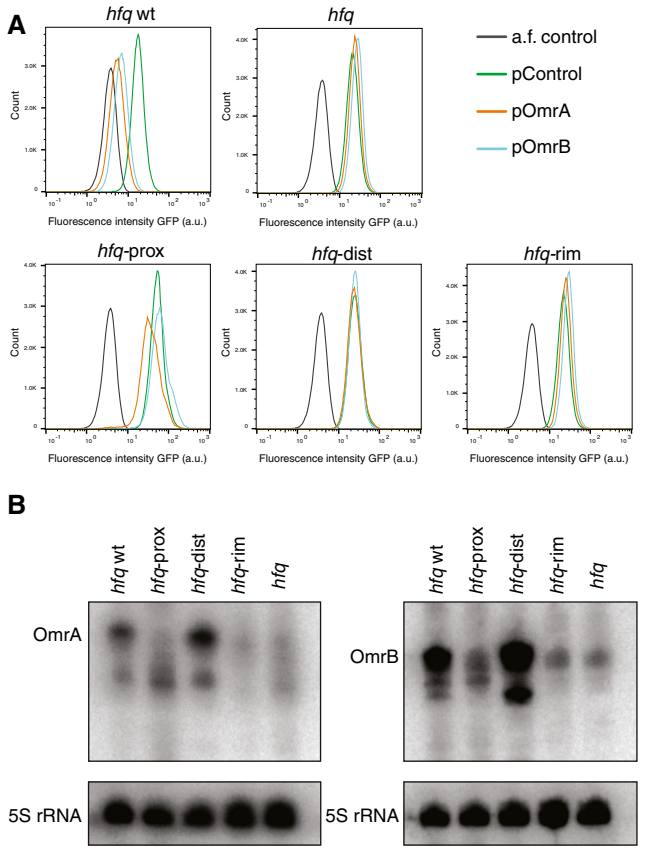

Figure 7. The Hfq distal face is essential for OmrA/B-dependent regulation of *dgcM in vivo*.

A Histograms show flow cytometry analysis of exponentially growing cells of *Escherichia coli* strain MC4100 *relA*⁻, and its mutant derivatives *hfq*-F42A (*hfq*-prox), *hfq*-Y25D (*hfq*-dist), *hfq*-R16S_R17A_R19A_K47E (*hfq*-rim), Δ*hfq*, harboring the translational fusion plasmid pDgcM::GFP in combination with pOmrA, pOmrB, or a control vector. Data were obtained on a MACSQuant VYB instrument.

B Northern blot analysis of total RNA isolated from the same cultures at the same time point as used for flow cytometry, probed for OmrA (strains containing pOmrA) or OmrB (strains containing pOmrB). 5S rRNA was used as loading control.

(Fig 2A and C), is partially sequestered in a stem–loop (Fig 4). This suggested a role for Hfq as an RNA remodeler to facilitate OmrA/B binding. The Hfq-binding site was mapped upstream of the *dgcM* SD and AUG, located opposite of sRNA site 1 in the local structure (Fig 4B). Indeed, an enhanced T1 cleavage of *dgcM* nucleotides G101 and G102 was observed when Hfq was bound, indicative of stem–loop destabilization (Fig 4). These residues became protected upon OmrA/B binding. *In vitro* translation experiments with *dgcM* mRNA, in presence or absence of OmrA/B, and with inclusion of wt or Hfq mutant proteins, pointed toward a requirement of Hfq distal face binding to the *dgcM* mRNA for OmrA/B-dependent inhibition (Fig 6A). By contrast, mutations in the proximal or rim surfaces had only minor effects on regulatory efficiency. From this, we infer that the predominant role of Hfq—in this case—lies in RNA structure remodeling. Strikingly, when this protein was substituted by an Hfq-mimic oligo, which base-paired to the mapped Hfq-binding site in *dgcM* mRNA, it restored inhibition by OmrA and OmrB in complete absence of Hfq (Fig 6B). Qualitatively supporting the above conclusions, binding rate determinations showed that oligo-bound *dgcM* mRNA indeed was more readily accessible to OmrA binding than the free mRNA (Appendix Fig S8). However, the only ≈three-fold effect measured and the low association rates obtained do not quantitatively match the stronger effects seen in the translation assay (Fig 6B). At this point, this discrepancy is unexplained but may be related to the different assay conditions—a single-step reaction (Appendix Fig S8) versus inhibition in multiple rounds of translation (Fig 6B). Supporting the *in vitro* translation results (Fig 6A), a distal face mutant Hfq was unable to support OmrA/B-dependent regulation of *dgcM::gfp in vivo*, even though the sRNA levels were high (Fig 7A and B). For the proximal and rim Hfq mutant, the *in vitro* and *in vivo* results differed, which however is readily explained. The two corresponding mutant strains fail to accumulate high sRNA levels (Fig 7B), as has been observed for many class 1 sRNAs (e.g., Schu *et al*, 2015), which results in loss of regulation. We conclude that, in contrast to several other mRNA-sRNA pairs, OmrA/B-*dgcM* mRNA complex formation relies on Hfq distal face binding both *in vitro* and *in vivo*, causing a subsequent restructuring of the *dgcM* mRNA, to facilitate OmrA/B association. Based on our *in vitro* results (Fig 6A), proximal and rim interactions contribute only marginally to regulation.

The capability of the RNA chaperone Hfq to locally unwind and/or restructure bound RNAs is well established and hardly surprising (e.g., Woodson *et al*, 2018). Remodeling has been demonstrated for the sRNAs OxyS, RprA, and DsrA (Zhang *et al*, 2002; Vecerek *et al*, 2008; Ribeiro Ede *et al*, 2012; Henderson *et al*, 2013), as well as the *ompA*, *sodB,* and *mutS* mRNAs (Moll *et al*, 2003b; Geissmann & Touati, 2004; Chen & Gottesman, 2017). In the case of *mutS,* Hfq inhibits translation through both sRNA-dependent and sRNA-independent mechanisms. While the sRNA ArcZ inhibits translation by base-pairing to the *mutS* 5′UTR, Hfq distal face binding remodels the mRNA leader to induce an inhibitory structure in the translation initiation region (Chen & Gottesman, 2017). However, these structural changes do not seem to affect inhibition of *mutS* by its regulator ArcZ; downregulation by ArcZ is almost as strong in an Hfq distal face mutant strain as in the wild-type (Chen & Gottesman, 2017).

Hfq-dependent remodeling of mRNA as a requirement for sRNA interaction has specifically been proposed for RyhB regulation of *sodB* (Geissmann & Touati, 2004). We noted however that, while Hfq-dependent structure remodeling of the *sodB* mRNA was demonstrated, the expected faster binding of RyhB to *sodB* mRNA in the presence of Hfq has not been experimentally tested. Neither has the effect of Hfq on translation initiation, or overall translation, been examined, thus rendering the mechanistic interpretations ambiguous (Geissmann & Touati, 2004). Moreover, the conclusions from this publication are at odds with another study of the same sRNA-target system (Hao *et al*, 2011). Here, a truncated RyhB variant, RyhBt, which is entirely Hfq-independent and stable in the absence of Hfq, was fully active in *sodB* expression control *in vivo*. Thus, whether remodeling of *sodB* mRNA is the critical event for regulation by RyhB, as proposed in Geissmann and Touati (2004), needs to be addressed by further experiments. Hfq-induced structural changes have also been reported for *ompA* mRNA, but it remains unknown whether they are required for duplex formation with targeting sRNAs (Moll *et al*, 2003b).

The *cis*-encoded RNA-IN and RNA-OUT system (transposon *Tn*10/*IS*10) also involves secondary structure rearrangements brought about by Hfq binding, suggested to explain how Hfq facilitates RNA-IN:OUT pairing (Ross *et al*, 2013). So far, the functional implications of these rearrangements are not entirely clear, in particular since an Hfq-independent binding pathway involving kissing loop interactions is known (Ross *et al*, 2013), and protein-free association rate constants of RNA-IN and RNA-OUT (0.5×10^6 M^{-1} s^{-1}; Ma & Simons, 1990) are > 100-fold faster than those typical for *trans*-encoded sRNAs (Wagner & Romby, 2015). This is different from our model, in that functional OmrA/B-*dgcM* mRNA interactions barely occur in the absence of Hfq (Appendix Fig S7). Though we propose that *dgcM*-OmrA/B is a first case in which this mechanism has been experimentally validated, other systems, like those above and others, may indeed work similarly. For example, regulation of *dgcM* mRNA by RprA (Mika *et al*, 2012) appears to occur at a binding site close to that of OmrA/B, and hence might conform to the same model.

A surprising finding was the ability of OmrA/B to protect *dgcM* mRNA from *in vitro* cleavage at two distinct but adjacent sites (Fig 4). Two-site recognition by one sRNA has previously been reported for the *lpxR* and *nhaB* mRNAs. In both cases, binding to one site overlapping the RBS blocks translation by competing with initiating ribosomes, whereas binding to the second site far downstream in the coding region induces RNase E-mediated cleavage (Corcoran *et al*, 2012; Chao & Vogel, 2016). Here, only OmrA/B binding site 1 (nt 88–102) in *dgcM* is associated with inhibition (Fig 3A and B) since mutations that weaken this interaction suffice to abolish regulation *in vivo* (Fig 2A and C). In light of these data, a regulatory role for site 2 seems unlikely.

In conclusion, the present analysis identified OmrA/B as regulators of yet another target within the biofilm pathway of *E. coli*, DgcM. More importantly, we uncovered a different and new mechanism of action for Hfq. Instead of acting as a canonical platform for simultaneous sRNA-mRNA binding, Hfq acts here—exclusively or at least primarily—by opening a local target structure in the *dgcM* mRNA to provide access to the regulatory sRNAs. The *in vitro* data strongly support these conclusions, although it cannot be ruled out that, e.g., a platform role of Hfq may contribute to *in vivo* activity. We suggest that it might be fruitful to search for similar examples of Hfq-dependent regulation in which this protein's RNA structure-remodeling activity, rather than its annealing function or duplex-stabilizing effect, plays the dominant role.

Materials and Methods

Chemicals, reagents, and oligodeoxyribonucleotides

Growth media components were purchased from Oxoid. Oligodeoxyribonucleotides/primers (Appendix Table S1) and chemicals were purchased from Sigma-Aldrich, and reagents from Thermo Fisher Scientific.

Growth conditions

Bacterial cells were grown aerobically at 37°C in L Broth. When applicable, antibiotics were added at 100 (ampicillin), 50 (kanamycin), or 15 μg/ml (chloramphenicol and tetracycline). For detection of curli expression, Congo Red plates (LA plates without NaCl, 20 μg/ml Congo red, 10 μg/ml Coomassie Brilliant Blue G) were used. Plates were incubated at 28°C for 24 h.

Bacterial strains and plasmids

All strains used in this study are derivatives of *E. coli* K12 MC4100 *relA*$^+$, unless otherwise stated. Strains and plasmids are listed in Appendix Tables S2 and S3, respectively.

Plasmids pOmrA, pOmrB, and pControl were previously published (Holmqvist *et al*, 2010). Plasmid pDgcM::GFP was constructed by inserting a *Nsi*I/*Nhe*I-digested PCR product (primers EHO-759/EHO-760) into *Nsi*I/*Nhe*I-digested pXG10-SF, fusing 641 bp from the transcription start site to *gfp*. pXG10-SF is identical to pXG-10 (Urban & Vogel, 2007) except for substitution of *gfp* by *sfgfp*. Plasmid pDgcM::3xFLAG was created by insertion of *dgcM::*3xFLAG between the *lac* promoter sequence and the terminator sequence on the pXG-10 vector, thereby replacing *gfp*: the *dgcM*::3xFLAG fragment was amplified from pET52-b_dgcM_FLAG (see below) with primers MHO-259 and MHO-260, introducing *Xba*I and *Pst*I restriction sites, and after digestion with both enzymes, ligated into *Xba*I/*Nsi*I digested pXG-10. Plasmids pOmrA_M2 and pOmrB_M2 were created using inverse PCR mutagenesis, with the desired mutations included in the primers (MHO-221/MHO-223 for OmrA/OmrB, respectively, and MHO-222). Briefly, after PCR amplification with the phosphorylated primers, pOmrA or pOmrB template DNA was digested by *Dpn*I, PCR product was purified (GeneJET PCR Purification Kit Thermo Fisher Scientific) and religated with Ready-to-go T4 ligase (Amersham). The pDgcM_M2::3xFLAG plasmid was created with primers MHO-217 and MHO-218 on pDgcM::3xFLAG as template. To create a Δ*dgcM* strain, *dgcM* was replaced by a FRT-flanked Amp^R cassette by Lambda Red recombination (Yu *et al*, 2000) using primers MHO-094 and MHO-095. For *dgcM* transcription, a plasmid with a T7-promoter, *dgcM* ORF, a FLAG-tag, and T7-terminator was constructed (pET52-b_dgcM_FLAG) from the pET52-b vector (Novagen) backbone, already carrying a T7-promoter and terminator sequence. The plasmid was linearized by PCR using primers MHO-238 and MHO-239, introducing a FLAG-tag and *Xho*I/*Aat*II restriction sites while deleting the His-tag and multiple cloning site. The *dgcM* 5′ UTR and ORF lacking its stop codon were PCR amplified with primers MHO-242/MHO-243, introducing *Xho*I/*Aat*II restriction sites. After digestion with both enzymes, vector and *dgcM* insert were ligated. *E. coli* Top10 cells were used for transformations (Invitrogen).

The *csgD:M4* and *ompR:mut2* mutations were introduced into strain MC4100 by Lambda red recombination (Yu *et al*, 2000) using plasmid pSim5-tet (Koskiniemi *et al*, 2011). First, a *kan-sacB* cassette (Pietsch *et al*, 2017), amplified with primers MHO-100/MHO-101 for *csgD:M4,* and MHO-268/MHO-269 for *ompR:mut2*, was inserted at the site of mutagenesis. A second round of recombination was done with a ssDNA fragment carrying the desired point mutation, followed by counterselection for SacB (Ellis *et al*, 2001). To create the double mutant, *ompR:mut2* was introduced into a wt as well as the *csgD:M4* background.

The F42A (prox) and Y25D (dist) *hfq* mutant strains were previously published (Zhang *et al*, 2013; Appendix Table S2). The R16S-R17A-R19A-K47E (rim) mutation, as well as an *hfq* deletion, was

introduced into the chromosome of the same MC4100 *relA*$^-$ strain background. This was done by replacing the *cat-sacB* cassette in MC4100 *relA*$^-$ Δ*hfq::cat-sacB* (Zhang *et al*, 2013), with a PCR fragment carrying the rim mutation, amplified from plasmid pETM60-St_Hfq102_R16S_R17A_R19A_K47E (Sauer *et al*, 2012) using primers MHO-294 and MHO-295, or with an oligo matching the *hfq* flanking region (MHO-291). The resulting strains were transformed with plasmids pDgcM::GFP and either pOmrA, pOmrB, or pControl.

Fluorescence measurements

For bulk measurements, bacterial cultures grown overnight from single colonies were diluted 1:100 in fresh LB medium and grown in 96-well black assay plates with clear flat bottom (Costar®) at 37°C. Fluorescence (GFP: excitation 480 nm, emission 520 nm) and optical density (600 nm) were measured for 23 h at 5-min intervals in a plate reader (Tecan Infinite Pro). Corrected fluorescence values were calculated as ratios between fluorescence and OD_{600}. To account for cellular auto-fluorescence, GFP/OD_{600} from a strain not expressing a fluorescent protein was subtracted. Background-subtracted GFP/OD_{600} values from each strain and time point were averaged and expressed relative to the corresponding strain transformed with the control plasmid lacking an sRNA gene.

Single-cell analysis of GFP fluorescence was conducted by flow cytometry on a MACSQuant® VYB instrument (Miltenyi Biotec). Cells were diluted in sterile-filtered PBS and loaded in a 96-well assay plate for analysis. GFP was excited with a blue laser (488 nm) in channel B1 (bandpass filter 525/50). For each sample, 100,000 events were recorded. The acquired data were processed with FlowJo software (FlowJo LLC) as follows. To exclude background noise, the events were first gated for bacterial cells based on side scatter measurements. Subsequently, the GFP fluorescence for the gated population was plotted as a histogram.

In vitro transcription of RNA

OmrA and OmrB DNA templates containing a T7 promoter, as well as a hammerhead ribozyme sequence, were generated as previously described (Holmqvist *et al*, 2010). OmrA_M2 was generated similarly using primers MHO-248 and MHO-249. To generate a 210 nt *dgcM* mRNA for structure probing and toeprinting assays, DNA templates containing a T7 promoter sequence were generated by PCR using primers MHO-159/MHO-194 with *E. coli* MC4100 *relA*$^+$ DNA as a template. The DNA templates were used for *in vitro* transcription using the Megascript Kit (Life Technologies, #AM1330). Transcription reactions were DNase I-treated (Roche) for 30 min at 37°C, followed by phenol–chloroform extraction and ethanol precipitation. RNAs were purified from denaturing polyacrylamide-urea gels by elution into 300 mM sodium acetate, 0.1% SDS, and 1 mM EDTA. After phenol–chloroform extraction, ethanol precipitation, washing with 80% ethanol, and drying, RNA was dissolved in TE buffer. RNA concentration and quality was assessed by NanoDrop and Denaturing PAGE.

5′ end-labeling was performed on CIAP-treated RNA (Invitrogen™, #18009-019) with T4 PNK (Thermo Fisher Scientific, #EK0031) and [γ-P^{32}]ATP (10 mCi/ml, 3,000 Ci/mmol). Labeled RNAs were gel-purified as above. Before use, RNAs were refolded in water for 1 min at 95°C followed by 1-min incubation on ice and renatured for 5 min at 37°C in renaturation buffer (100 mM K-acetate, 10 mM Mg-acetate, 50 mM HEPES-NaOH pH 7.5).

For *in vitro* translation assays, *ompA* and *dgcM* RNAs including C-terminal FLAG-tag and terminator sequences were used. PCR template for *ompA*-FLAG RNA transcription was generated using primers MHO-207 and MHO-230 from DNA of strain MC4100 *ompA-FLAG*. This strain was created by flipping the kanamycin resistance cassette out of strain E388 (Holmqvist *et al*, 2010) using the pCP20 plasmid. For *dgcM* transcription, the PCR fragment used contained the T7 promoter, the FLAG-tagged *dgcM* sequence, and a T7 terminator (template pET52b_dgcM_FLAG, primers MHO-244/MHO-245).

RNA secondary structure probing

Structural probing was carried out on 5′ end-labeled RNA. Reactions were performed at 37°C in the presence of 1 μg carrier yeast tRNA. When applicable, OmrA/B binding to *dgcM* RNA was allowed for 15 min in presence or absence of Hfq hexamers (50 nM). Enzymatic probing was done with 0.1 unit of RNAse T1 (Invitrogen™, #AM22®83) for 5 min, stopped by addition of cold Na-acetate (0.3 M), followed by phenol/chloroform/isoamyl alcohol (25/24/1) extraction. Chemical probing was done with lead(II) acetate at a final concentration of 5 mM for 5 min. Reactions were stopped with cold EDTA (50 mM final concentration). After precipitation, RNAs pellets were dried and dissolved in loading dye. Samples were resolved on 7.5% sequencing gels, fixed for 5 min (10% ethanol, 6% acetic acid), transferred to 3-mm Whatman paper, and dried. Signals were detected using a PhosphorImager screen and a PMI scanner™ (Bio-Rad).

Toeprinting assays

Final concentrations in 10 μl toeprinting reactions were 20 nM of mRNA and, when present, 100 nM of 30S subunits, 300 nM of initiator tRNA, and 0.5 mM of dNTPs. Briefly, mRNAs were denatured for 1 min at 90°C with radiolabeled primers and dNTPs in 1× RT-buffer (10 mM Tris acetate pH 7.6, 100 mM K-acetate, 1 mM DTT). After 1 min on ice, Mg-acetate was added to 10 mM final concentration. RNAs were refolded for 5 min, followed by addition of activated 30S (15 min at 37°C in 1× RT-buffer). After 10 min, initiator tRNA was added, and incubation continued for 25 min. Reverse transcription was started by addition of 100 U of SSIV (Invitrogen™, #18090010) for 20 min. Reactions were stopped by cold STOP buffer (50 mM Tris–HCl pH 7.5, 0.1% SDS, 10 mM EDTA). After phenol/chloroform extraction, the RNA template was removed by KOH treatment for 3 min at 95°C. After base neutralization with acetic acid, the cDNAs were ethanol-precipitated, centrifuged, dissolved in loading buffer, and resolved on 7.5% sequencing gels. Gels were fixed and treated as above.

Gel mobility shift assay

5′ end-labeled refolded RNA was incubated at various concentrations of unlabeled complementary RNA, in presence or absence of Hfq, for 30 min at 37°C. Reactions were stopped by adding loading dye (48% glycerol, 0.01% xylene cyanol, 0.01% bromophenol blue), and samples directly loaded on a 5% non-denaturing PA-gel. To avoid heat-induced duplex separation, gels were run at 4°C for 3 h (300 V) in 0.5× TEB. Gel transfer and analysis was as

above. When blocking oligonucleotides were used (Fig 5), they were included in the denaturation and refolding steps of the RNAs.

In vitro translation assay

In vitro translation assays (reaction volumes 10 μl) were done in the PURExpress® *In Vitro* Protein Synthesis Kit (New England BioLabs), with *dgcM* mRNA containing a FLAG-tag and terminator sequence. The *dgcM-FLAG* RNA was first diluted in 3 μl HMK (10 mM HEPES-NaOH pH 7.5, 10 mM Mg-acetate, 100 mM K-acetate). When indicated, *ompA-FLAG* RNA, OmrA or OmrB, and Hfq protein were included in this 3 μl volume. Final RNA concentrations were 10 nM *dgcM-FLAG*, 0.3 nM *ompA-FLAG*, and 500 nM OmrA or OmrB. Hfq protein was included at 18 nM (hexamer). The wild-type Hfq used was His-tagged, from *E. coli* strain BL21 (DE3)pLys with plasmid pTE607 (Fender *et al*, 2010). In Fig 6A, we used the functionally equivalent *Salmonella Typhimurium* Hfq proteins, wild-type or with mutations as indicated (St_Hfq102; wild-type), proximal (St_Hfq102_F42A), distal (St_Hfq102_Y25A_Q52A), or rim (St_Hfq 1 02-R1 6S-R1 7A-R1 9A-K47 E; Sauer *et al*, 2012). The Hfq-mimic oligo (Hfq_BS; Appendix Table S1) used in Fig 6B was used at a final concentration of 50 nM.

RNAs and Hfq were pre-incubated for 5 min at 37°C before adding 7 μl of pre-mixed PURExpress solution A (4 μl) and B (3 μl). After 30 min at 37°C, 2.5 μl of 4× Laemmli sample buffer (Bio-Rad) was added, on ice. Detection of 3xFLAG-tagged DgcM and OmpA protein products was as described below.

Western blot analysis

Aliquots were withdrawn from cultures at OD_{600} of 0.3 and 0.5, spun down, and pellets resuspended in 1× loading dye [4× Laemmli sample buffer (Bio-Rad), 1/10 volume of β-mercaptoethanol added before use]. Samples were incubated for 5 min at 95°C before gel electrophoresis. Proteins were separated on an Any kD™ Mini-PROTEAN® TGX Stain-Free™ Gel (Bio-Rad), followed by fluorescent detection of total protein by ChemiDoc™ MP (Bio-Rad) and the "Any kD™ Mini-PROTEAN® TGX Stain-Free™ Gel" application. Then, proteins were transferred to a PVDF membrane with the Trans-Blot Turbo™ Mini PVDF transfer Packs (Bio-Rad) and the Trans-Blot Turbo Transfer System (Bio-Rad) using the "Any Kd" preset. After o/n blocking in Odyssey® Blocking Buffer (PBS; LI-COR) at 4°C, membranes were incubated for 1 h with monoclonal ANTI-FLAG M2-Peroxidase (HRP) mouse antibody (Sigma; cat. nr. A8592) at r.t., followed by three washes with PBS-T, and two with PBS. Blots were developed with Amersham™ ECL™ Prime Western Blotting Detection Reagent (GE Healthcare) and imaged using ChemiDoc™ MP (Bio-Rad) with Chemi Hi Resolution application. Images were analyzed with Image Lab Software (version 4.0 build 16); the quantification of band intensities in Fig 6 used equal-sized squares and pixel counts for background, DgcM, and OmpA.

Northern blot analysis

Samples of exponential-phase liquid cultures were withdrawn and mixed with 0.25 volume of stop solution (95% ethanol, 5% phenol). Cells were pelleted by centrifugation and frozen in liquid nitrogen. After thawing on ice, total RNA was isolated by the hot acid-phenol method (Blomberg *et al*, 1990). 5 μg of extracted total RNA was mixed with 2× RNA loading buffer [95% (v/v) formamide, 0.025% (w/v) bromophenol blue, 0.025% (w/v) xylene cyanol], heated for 2 min at 95°C, and separated on an 8% sequencing gel. After electrophoresis (Bio-Rad Trans-Blot cell), RNA was transferred to an Amersham Hybond™-N+ membrane (GE Healthcare) by electro-blotting, and UV-crosslinked. 5′-end-labeled oligodeoxyribonucleotide probes were used for detection of OmrA (EHO-406), OmrB (EHO-407) and, as loading control, 5S rRNA (EHO-690). Prehybridization and hybridization of the membrane were carried out in modified Church and Gilbert hybridization buffer (Church & Gilbert, 1984), at 42°C. For visualization of bands, a Personal Molecular Imager (PMI—Bio-Rad) was used.

Expanded View for this article is available online.

Acknowledgements
We are grateful to Evelyn Sauer and Oliver Weichenrieder for purified Hfq proteins and plasmids, and to Gisela Storz and Aixia Zhang for providing us with *hfq* mutants strains. Initiator tRNA was a generous gift from Suparna Sanyal. We acknowledge support from The Swedish Research Council (to E.G.H. Wagner).

Author contributions
MH and CR conducted the experimental work. MH, CR, EH, and EGHW planned the work, evaluated the data, and wrote the manuscript.

Conflict of interest
The authors declare that they have no conflict of interest.

References

Argaman L, Hershberg R, Vogel J, Bejerano G, Wagner EGH, Margalit H, Altuvia S (2001) Novel small RNA-encoding genes in the intergenic regions of *Escherichia coli*. *Curr Biol* 11: 941 – 950

Barquist L, Vogel J (2015) Accelerating discovery and functional analysis of small RNAs with new technologies. *Annu Rev Genet* 49: 367 – 394

Beich-Frandsen M, Vecerek B, Sjöblom B, Bläsi U, Djinović-Carugo K (2011) Structural analysis of full-length Hfq from *Escherichia coli*. *Acta Crystallogr Sect F Struct Biol Cryst Commun* 67: 536 – 540

Beisel CL, Storz G (2010) Base pairing small RNAs and their roles in global regulatory networks. *FEMS Microbiol Rev* 34: 866 – 882

Blomberg P, Wagner EGH, Nordström K (1990) Control of replication of plasmid R1: the duplex between the antisense RNA, CopA, and its target, CopT, is processed specifically *in vivo* and *in vitro* by RNaseIII. *EMBO J* 9: 2331 – 2340

Boehm A, Kaiser M, Li H, Spangler C, Kasper CA, Ackermann M, Kaever V, Sourjik V, Roth V, Jenal U (2010) Second messenger-mediated adjustment of bacterial swimming velocity. *Cell* 141: 107 – 116

Bordeau V, Felden B (2014) Curli synthesis and biofilm formation in enteric bacteria are controlled by a dynamic small RNA module made up of a pseudoknot assisted by an RNA chaperone. *Nucleic Acids Res* 42: 4682 – 4696

Bouvier M, Sharma CM, Mika F, Nierhaus KH, Vogel J (2008) Small RNA binding to 5′ mRNA coding region inhibits translational initiation. *Mol Cell* 32: 827 – 837

Brosse A, Korobeinikova A, Gottesman S, Guillier M (2016) Unexpected properties of sRNA promoters allow feedback control via regulation of a two-component system. *Nucleic Acids Res* 44: 9650 – 9666

Busch A, Richter AS, Backofen R (2008) IntaRNA: efficient prediction of bacterial sRNA targets incorporating target site accessibility and seed regions. *Bioinformatics* 24: 2849 – 2856

Carrier M-C, Lalaouna D, Massé E (2018) Broadening the definition of bacterial small RNAs: characteristics and mechanisms of action. *Annu Rev Microbiol* 72: 141 – 161

Chao Y, Papenfort K, Reinhardt R, Sharma CM, Vogel J (2012) An atlas of Hfq-bound transcripts reveals 3′ UTRs as a genomic reservoir of regulatory small RNAs. *EMBO J* 31: 4005 – 4019

Chao Y, Vogel J (2016) A 3′ UTR-derived small RNA provides the regulatory noncoding arm of the inner membrane stress response. *Mol Cell* 61: 352 – 363

Chen J, Gottesman S (2017) Hfq links translation repression to stress-induced mutagenesis in *E. coli*. *Genes Dev* 31: 1382 – 1395

Church GM, Gilbert, (1984) Genomic sequencing. *Proc Natl Acad Sci USA* 81: 1991 – 1995

Colgan AM, Kröger C, Diard M, Hardt W-D, Puente JL, Sivasankaran SK, Hokamp K, Hinton JCD (2016) The impact of 18 ancestral and horizontally-acquired regulatory proteins upon the transcriptome and sRNA landscape of *Salmonella enterica* serovar Typhimurium. *PLoS Genet* 12: e1006258

Corcoran CP, Podkaminski D, Papenfort K, Urban JH, Hinton JCD, Vogel J (2012) Superfolder GFP reporters validate diverse new mRNA targets of the classic porin regulator, MicF RNA. *Mol Microbiol* 84: 428 – 445

De Lay N, Gottesman S (2012) A complex network of small non-coding RNAs regulate motility in *Escherichia coli*. *Mol Microbiol* 86: 524 – 538

Dimastrogiovanni D, Fröhlich KS, Bandyra KJ, Bruce HA, Hohensee S, Vogel J, Luisi BF (2014) Recognition of the small regulatory RNA RydC by the bacterial Hfq protein. *eLife* 3: e05375

Ellis HM, Yu D, DiTizio T, Court DL (2001) High efficiency mutagenesis, repair, and engineering of chromosomal DNA using single-stranded oligonucleotides. *Proc Natl Acad Sci USA* 98: 6742 – 6746

Fender A, Elf J, Hampel K, Zimmermann B, Wagner EGH (2010) RNAs actively cycle on the Sm-like protein Hfq. *Genes Dev* 24: 2621 – 2626

Geissmann TA, Touati D (2004) Hfq, a new chaperoning role: binding to messenger RNA determines access for small RNA regulator. *EMBO J* 23: 396 – 405

Gerstel U, Park C, Römling U (2003) Complex regulation of csgD promoter activity by global regulatory proteins. *Mol Microbiol* 49: 639 – 654

Gorski SA, Vogel J, Doudna JA (2017) RNA-based recognition and targeting: sowing the seeds of specificity. *Nat Rev Mol Cell Biol* 18: 215 – 228

Gottesman S, Storz G (2011) Bacterial small RNA regulators: versatile roles and rapidly evolving variations. *Cold Spring Harb Perspect Biol* 3: a003798

Guillier M, Gottesman S (2006) Remodelling of the *Escherichia coli* outer membrane by two small regulatory RNAs. *Mol Microbiol* 59: 231 – 247

Guillier M, Gottesman S (2008) The 5′ end of two redundant sRNAs is involved in the regulation of multiple targets, including their own regulator. *Nucleic Acids Res* 36: 6781 – 6794

Hammar M, Arnqvist A, Bian Z, Olsén A, Normark S (1995) Expression of two csg operons is required for production of fibronectin- and congo red-binding curli polymers in *Escherichia coli* K-12. *Mol Microbiol* 18: 661 – 670

Hao Y, Zhang ZJ, Erickson DW, Huang M, Huang Y, Li J, Hwa T, Shi H (2011) Quantifying the sequence-function relation in gene silencing by bacterial small RNAs. *Proc Natl Acad Sci USA* 108: 12473 – 12478

Henderson CA, Vincent HA, Casamento A, Stone CM, Phillips JO, Cary PD, Sobott F, Gowers DM, Taylor JE, Callaghan AJ (2013) Hfq binding changes the structure of *Escherichia coli* small noncoding RNAs OxyS and RprA, which are involved in the riboregulation of rpoS. *RNA* 19: 1089 – 1104

Hengge R, Galperin MY, Ghigo J-M, Gomelsky M, Green J, Hughes KT, Jenal U, Landini P (2015) Systematic nomenclature for GGDEF and EAL domain-containing cyclic Di-GMP turnover proteins of *Escherichia coli*. *J Bacteriol* 198: 7 – 11

Holmqvist E, Reimegård J, Sterk M, Grantcharova N, Römling U, Wagner EGH (2010) Two antisense RNAs target the transcriptional regulator CsgD to inhibit curli synthesis. *EMBO J* 29: 1840 – 1850

Holmqvist E, Wright PR, Li L, Bischler T, Barquist L, Reinhardt R, Backofen R, Vogel J (2016) Global RNA recognition patterns of post-transcriptional regulators Hfq and CsrA revealed by UV crosslinking *in vivo*. *EMBO J* 35: 991 – 1011

Holmqvist E, Wagner EGH (2017) Impact of bacterial sRNAs in stress responses. *Biochem Soc Trans* 45: 1203 – 1212

Holmqvist E, Vogel J (2018) RNA-binding proteins in bacteria. *Nat Rev Microbiol* 16: 601 – 615

Hussein R, Lim HN (2011) Disruption of small RNA signaling caused by competition for Hfq. *Proc Natl Acad Sci USA* 108: 1110 – 1115

Ishikawa H, Otaka H, Maki K, Morita T, Aiba H (2012) The functional Hfq-binding module of bacterial sRNAs consists of a double or single hairpin preceded by a U-rich sequence and followed by a 3′ poly(U) tail. *RNA* 18: 1062 – 1074

Jagodnik J, Chiaruttini C, Guillier M (2017) Stem-loop structures within mRNA coding sequences activate translation initiation and mediate control by small regulatory RNAs. *Mol Cell* 68: 158 – 170

Jørgensen MG, Nielsen JS, Boysen A, Franch T, Møller-Jensen J, Valentin-Hansen P (2012) Small regulatory RNAs control the multi-cellular adhesive lifestyle of *Escherichia coli*. *Mol Microbiol* 84: 36 – 50

Koskiniemi S, Pränting M, Gullberg E, Näsvall J, Andersson DI (2011) Activation of cryptic aminoglycoside resistance in *Salmonella enterica*. *Mol Microbiol* 80: 1464 – 1478

Lalaouna D, Simoneau-Roy M, Lafontaine D, Massé E (2013) Regulatory RNAs and target mRNA decay in prokaryotes. *Biochim Biophys Acta* 1829: 742 – 747

Lease RA, Woodson SA (2004) Cycling of the Sm-like protein Hfq on the DsrA small regulatory RNA. *J Mol Biol* 344: 1211 – 1223

Lévi-Meyrueis C, Monteil V, Sismeiro O, Dillies M-A, Monot M, Jagla B, Coppée J-Y, Dupuy B, Norel F (2014) Expanding the RpoS/σS-network by RNA sequencing and identification of σS-controlled small RNAs in *Salmonella*. *PLoS One* 9: e96918

Lindenberg S, Klauck G, Pesavento C, Klauck E, Hengge R (2013) The EAL domain protein YciR acts as a trigger enzyme in a c-di-GMP signalling cascade in *E. coli* biofilm control. *EMBO J* 32: 2001 – 2014

Link TM, Valentin-Hansen P, Brennan RG (2009) Structure of *Escherichia coli* Hfq bound to polyriboadenylate RNA. *Proc Natl Acad Sci USA* 106: 19292 – 19297

Ma C, Simons RW (1990) The IS10 antisense RNA blocks ribosome binding at the transposase translation initiation site. *EMBO J* 9: 1267 – 1274

Melamed S, Peer A, Faigenbaum-Romm R, Gatt YE, Reiss N, Bar A, Altuvia Y, Argaman L, Margalit H (2016) Global mapping of small RNA-target interactions in bacteria. *Mol Cell* 63: 884 – 897

Mika F, Busse S, Possling A, Berkholz J, Tschowri N, Sommerfeldt N, Pruteanu M, Hengge R (2012) Targeting of csgD by the small regulatory RNA RprA links stationary phase, biofilm formation and cell envelope stress in *Escherichia coli*. *Mol Microbiol* 84: 51 – 65

Mika F, Hengge R (2013) Small regulatory RNAs in the control of motility and biofilm formation in *E. coli* and *Salmonella*. *Int J Mol Sci* 14: 4560 – 4579

Mika F, Hengge R (2014) Small RNAs in the control of RpoS, CsgD, and biofilm architecture of *Escherichia coli*. *RNA Biol* 11: 494 – 507

Moll I, Afonyushkin T, Vytvytska O, Kaberdin VR, Bläsi U (2003a) Coincident Hfq binding and RNase E cleavage sites on mRNA and small regulatory RNAs. *RNA* 9: 1308 – 1314

Moll I, Leitsch D, Steinhauser T, Bläsi U (2003b) RNA chaperone activity of the Sm-like Hfq protein. *EMBO Rep* 4: 284 – 289

Møller T, Franch T, Højrup P, Keene DR, Bächinger HP, Brennan RG, Valentin-Hansen P (2002) Hfq: a bacterial Sm-like protein that mediates RNA-RNA interaction. *Mol Cell* 9: 23 – 30

Moon K, Gottesman S (2011) Competition among Hfq-binding small RNAs in *Escherichia coli*. *Mol Microbiol* 82: 1545 – 1562

Ogasawara H, Yamada K, Kori A, Yamamoto K, Ishihama A (2010) Regulation of the *Escherichia coli* csgD promoter: interplay between five transcription factors. *Microbiology* 156: 2470 – 2483

Olejniczak M (2011) Despite similar binding to the Hfq protein regulatory RNAs widely differ in their competition performance. *Biochemistry* 50: 4427 – 4440

Otaka H, Ishikawa H, Morita T, Aiba H (2011) PolyU tail of rho-independent terminator of bacterial small RNAs is essential for Hfq action. *Proc Natl Acad Sci USA* 108: 13059 – 13064

Panja S, Schu DJ, Woodson SA (2013) Conserved arginines on the rim of Hfq catalyze base pair formation and exchange. *Nucleic Acids Res* 41: 7536 – 7546

Panja S, Paul R, Greenberg MM, Woodson SA (2015) Light-triggered RNA annealing by an RNA chaperone. *Angew Chem Int Ed Engl* 54: 7281 – 7284

Papenfort K, Sun Y, Miyakoshi M, Vanderpool CK, Vogel J (2013) Small RNA-mediated activation of sugar phosphatase mRNA regulates glucose homeostasis. *Cell* 153: 426 – 437

Papenfort K, Vanderpool CK (2015) Target activation by regulatory RNAs in bacteria. *FEMS Microbiol Rev* 39: 362 – 378

Peano C, Wolf J, Demol J, Rossi E, Petiti L, De Bellis G, Geiselmann J, Egli T, Lacour S, Landini P (2015) Characterization of the *Escherichia coli* σ(S) core regulon by chromatin immunoprecipitation-sequencing (ChIP-seq) analysis. *Sci Rep* 5: 10469

Peng Y, Curtis JE, Fang X, Woodson SA (2014a) Structural model of an mRNA in complex with the bacterial chaperone Hfq. *Proc Natl Acad Sci USA* 111: 17134 – 17139

Peng Y, Soper TJ, Woodson SA (2014b) Positional effects of AAN motifs in rpoS regulation by sRNAs and Hfq. *J Mol Biol* 426: 275 – 285

Pietsch F, Bergman JM, Brandis G, Marcusson LL, Zorzet A, Huseby DL, Hughes D (2017) Ciprofloxacin selects for RNA polymerase mutations with pleiotropic antibiotic resistance effects. *J Antimicrob Chemother* 72: 75 – 84

Prigent-Combaret C, Brombacher E, Vidal O, Ambert A, Lejeune P, Landini P, Dorel C (2001) Complex regulatory network controls initial adhesion and biofilm formation in *Escherichia coli* via regulation of the csgD gene. *J Bacteriol* 183: 7213 – 7223

Rajkowitsch L, Schroeder R (2007) Dissecting RNA chaperone activity. *RNA* 13: 2053 – 2060

Ribeiro Ede A Jr, Beich-Frandsen M, Konarev PV, Shang W, Vecerek B, Kontaxis G, Hämmerle H, Peterlik H, Svergun DI, Bläsi U, Djinović-Carugo K (2012) Structural flexibility of RNA as molecular basis for Hfq chaperone function. *Nucleic Acids Res* 40: 8072 – 8084

Robinson KE, Orans J, Kovach AR, Link TM, Brennan RG (2014) Mapping Hfq-RNA interaction surfaces using tryptophan fluorescence quenching. *Nucleic Acids Res* 42: 2736 – 2749

Römling U, Sierralta WD, Eriksson K, Normark S (1998) Multicellular and aggregative behaviour of *Salmonella typhimurium* strains is controlled by mutations in the agfD promoter. *Mol Microbiol* 28: 249 – 264

Römling U (2005) Characterization of the rdar morphotype, a multicellular behaviour in Enterobacteriaceae. *Cell Mol Life Sci* 62: 1234 – 1246

Ross JA, Ellis MJ, Hossain S, Haniford DB (2013) Hfq restructures RNA-IN and RNA-OUT and facilitates antisense pairing in the Tn10/IS10 system. *RNA* 19: 670 – 684

Salim NN, Feig AL (2010) An upstream Hfq binding site in the fhlA mRNA leader region facilitates the OxyS-fhlA interaction. *PLoS One* 5: e13028

Santiago-Frangos A, Kavita K, Schu DJ, Gottesman S, Woodson SA (2016) C-terminal domain of the RNA chaperone Hfq drives sRNA competition and release of target RNA. *Proc Natl Acad Sci USA* 113: E6089 – E6096

Santiago-Frangos A, Woodson SA (2018) Hfq chaperone brings speed dating to bacterial sRNA. *Wiley Interdiscip Rev RNA* 9: e1475

Sauer E, Weichenrieder O (2011) Structural basis for RNA 3′-end recognition by Hfq. *Proc Natl Acad Sci USA* 108: 13065 – 13070

Sauer E, Schmidt S, Weichenrieder O (2012) Small RNA binding to the lateral surface of Hfq hexamers and structural rearrangements upon mRNA target recognition. *Proc Natl Acad Sci USA* 109: 9396 – 9401

Schu DJ, Zhang A, Gottesman S, Storz G (2015) Alternative Hfq-sRNA interaction modes dictate alternative mRNA recognition. *EMBO J* 34: 2557 – 2573

Sharma CM, Darfeuille F, Plantinga TH, Vogel J (2007) A small RNA regulates multiple ABC transporter mRNAs by targeting C/A-rich elements inside and upstream of ribosome-binding sites. *Genes Dev* 21: 2804 – 2817

Thomason MK, Fontaine F, De Lay N, Storz G (2012) A small RNA that regulates motility and biofilm formation in response to changes in nutrient availability in *Escherichia coli*. *Mol Microbiol* 84: 17 – 35

Tree JJ, Granneman S, McAteer SP, Tollervey D, Gally DL (2014) Identification of bacteriophage-encoded anti-sRNAs in pathogenic *Escherichia coli*. *Mol Cell* 55: 199 – 213

Updegrove TB, Zhang A, Storz G (2016) Hfq: the flexible RNA matchmaker. *Curr Opin Microbiol* 30: 133 – 138

Urban JH, Vogel J (2007) Translational control and target recognition by *Escherichia coli* small RNAs *in vivo*. *Nucleic Acids Res* 35: 1018 – 1037

Vecerek B, Rajkowitsch L, Sonnleitner E, Schroeder R, Bläsi U (2008) The C-terminal domain of *Escherichia coli* Hfq is required for regulation. *Nucleic Acids Res* 36: 133 – 143

Vidal O, Longin R, Prigent-Combaret C, Dorel C, Hooreman M, Lejeune P (1998) Isolation of an *Escherichia coli* K-12 mutant strain able to form biofilms on inert surfaces: involvement of a new ompR allele that increases curli expression. *J Bacteriol* 180: 2442 – 2449

Vogel J, Bartels V, Tang TH, Churakov G, Slagter-Jäger JG, Hüttenhofer A, Wagner EGH (2003) RNomics in *Escherichia coli* detects new sRNA species and indicates parallel transcriptional output in bacteria. *Nucleic Acids Res* 31: 6435 – 6443

Vogel J, Argaman L, Wagner EGH, Altuvia S (2004) The small RNA IstR inhibits synthesis of an SOS-induced toxic peptide. *Curr Biol* 14: 2271 – 2276

Vogel J, Luisi BF (2011) Hfq and its constellation of RNA. *Nat Rev Microbiol* 9: 578 – 589

Wagner EGH (2013) Cycling of RNAs on Hfq. *RNA Biol* 10: 619 – 626

Wagner EGH, Altuvia S, Romby P (2002) Antisense RNAs in bacteria and their genetic elements. *Adv Genet* 46: 361 – 398

Wagner EGH, Romby P (2015) Small RNAs in bacteria and archaea: who they are, what they do, and how they do it. *Adv Genet* 90: 133 – 208

Wassarman KM, Repoila F, Rosenow C, Storz G, Gottesman S (2001) Identification of novel small RNAs using comparative genomics and microarrays. *Genes Dev* 15: 1637 – 1651

Waters LS, Storz G (2009) Regulatory RNAs in bacteria. *Cell* 136: 615 – 628

Woodson SA, Panja S, Santiago-Frangos A (2018) Proteins that chaperone RNA regulation. *Microbiol Spectr* 6. https://doi.org/10.1128/microbiolspec.rwr-0026-2018

Wroblewska Z, Olejniczak M (2016) Hfq assists small RNAs in binding to the coding sequence of ompD mRNA and in rearranging its structure. *RNA* 22: 979 – 994

Yu D, Ellis HM, Lee EC, Jenkins NA, Copeland NG, Court DL (2000) An efficient recombination system for chromosome engineering in *Escherichia coli*. *Proc Natl Acad Sci USA* 97: 5978 – 5983

Zhang A, Wassarman KM, Ortega J, Steven AC, Storz G (2002) The Sm-like Hfq protein increases OxyS RNA interaction with target mRNAs. *Mol Cell* 9: 11 – 22

Zhang A, Wassarman KM, Rosenow C, Tjaden BC, Storz G, Gottesman S (2003) Global analysis of small RNA and mRNA targets of Hfq. *Mol Microbiol* 50: 1111 – 1124

Zhang A, Schu DJ, Tjaden BC, Storz G, Gottesman S (2013) Mutations in interaction surfaces differentially impact *E. coli* Hfq association with small RNAs and their mRNA targets. *J Mol Biol* 425: 3678 – 3697

Zuker M (2003) Mfold web server for nucleic acid folding and hybridization prediction. *Nucleic Acids Res* 31: 3406 – 3415